Available online at www.sciencedirect.com
SCIENCE DIRECT®
International Journal of Refractory Metals & Hard Materials 24 (2006) 253–262
International Journal of REFRACTORY METALS & HARD MATERIALS
www.elsevier.com/locate/ijrmhm

Development of niobium powder injection molding: Part I. Feedstock and injection molding

Gaurav Aggarwal, Seong Jin Park, Ivi Smid *

Center for Innovative Sintered Products (CISP), The Pennsylvania State University, 147 Research West, University Park, PA 16802-6809, USA

Received 26 March 2005; accepted 21 June 2005

Abstract

It has been only during the past four decades that niobium has been consumed on an industrial scale. Pure niobium and niobium base alloys constitute less than 2% of the global niobium market. Niobium being a refractory metal doesn't have a powder cost penalty as in ferrous materials, since refractory parts are formed from powders. This article details a systematical approach to develop feedstock for powder injection molding of niobium. It has been proven that powder injection molding is a viable forming technique for pure niobium. Further, rheological properties have been combined to determine optimal and critical solids loading. Based on simulation, injection temperatures and pressures were determined for optimal filling time. For the first time, a processing window has been identified based on the rheological behavior and simulation of niobium feedstock.

Keywords: Powder injection molding of niobium; Nb powder and feedstock; Rheological properties of niobium; Shear viscosity; Optimum filling time and PIM parameters; Moldability index; Critical solids loading

1. Introduction

Niobium was discovered in 1801 by the British chemist Charles Hatchett, who called it columbium. The present name was given by the German chemist Heinrich Rose, who separated it from tantalum. Like tantalum, niobium is a body-centered cubic, soft, and ductile material which can be worked and machined easily if it contains no impurities. Although niobium was discovered 200 years ago, it took its meaningful place, both in industry and history only after large deposits in Canada and Brazil were discovered in the mid 1950s. Over 80% of the world supply of niobium comes from Brazil's mineral reserves [1–3]. The majority of niobium is used in steels since its present position is uncontested in the three main microalloyed steel domains—pipe, automotive and structural. Niobium as a microalloying element in steels inhibits recrystallization by pinning the grain boundaries, suppresses austenite to ferrite transformation, and helps in precipitation strengthening [4]. Niobium is accepted as a key alloying element in a number of major nickel-base superalloys because of its potential to strengthen an alloy by solid solution strengthening, carbide formation, and by coherent precipitation hardening phase formation [5]. To improve the properties of cemented carbides, niobium carbide (NbC) is used as an additive. It is added in significant amounts where high temperatures and high loads are generated in operation, where abrasive wear resistance is of secondary importance, and where high-temperature reaction with iron-based material is of concern [6].

But there are many niobium-base alloys, too. Nb–47%Ti is a well-known alloy used in superconducting magnets, as its electrical resistance disappears if the metal is cooled below −264 °C. This is the highest transition temperature of all metals. These days, Nb–1%Zr

* Corresponding author. Tel.: +1 814 863 8208; fax: +1 814 863 8211.
E-mail address: smid@psu.edu (I. Smid).

0263-4368/$ - see front matter © 2005 Elsevier Ltd. All rights reserved.
doi:10.1016/j.ijrmhm.2005.06.003

is the prominent material of choice for critical metal parts in high-pressure-sodium (HPS) discharge lamps. This alloy has a high melting point and thermal conductivity, and thereby exhibits long life in a sodium vapor environment. The alloy found to have the most promising combination of elevated strength and fabrication characteristics is the C-103 alloy, which has a nominal composition of Nb–10%Hf–1%Ti [7]. More recently, niobium oxides have developed into an important material for some niche markets. NbO_2 is used in microelectronics for switching devices [8]. Nb_2O_5 can be used as a dielectric because of its high dielectric constant (11–100) or as an antireflection coating, because of its high refractive index (2.2–2.6) [9]. Niobium oxide is well established as a material for ceramic capacitors. Nb is also an attractive substitute for Ta in solid electrolytic capacitors because it is lighter and cheaper. In addition to that, the dielectric niobium pentoxide (Nb_2O_5) shows higher relative permittivity compared to tantalum pentoxide (Ta_2O_5) [10,11]. From the above discussion, niobium can be viewed as a versatile metal; it helps us to travel (aircraft turbine engines, magnetically levitated trains, automobiles), it facilitates in illuminating buildings (high pressure sodium vapor lamps), it is used in the medical field for its biocompatibility and corrosion resistance, and it helps in fabricating modern electronic gadgetry (lithium niobate I.F. filters, niobium capacitors).

All of the niobium alloys in production today were developed in the 1960s [12]. At that time, alloys were produced by common metal working processes such as forging, extrusion, spinning, and welding. Several attempts were also made to fabricate niobium by investment casting. This process was either limited to simple shapes or frequently beset by poor material utilization and contamination [13]. As a result, net-shaped processing techniques based on sintering of powders can provide an attractive route for overcoming such limitations. But particulate material processing routes received little attention during that time period because of limited knowledge of powder production methods. Recent studies in the production and sintering of niobium powders indicate that processing via near net-shape processing is feasible [14]. The most difficult aspect of processing niobium alloys by powder methods is preparation of the alloys into powder. These limitations arise due to the high melting points and reactive properties of the alloys. High-purity powders can only be produced by costly procedures such as the hydride–dehydride process and centrifugal atomization using electron beam or plasma as a heat source [15]. To overcome the disadvantage of high powder cost and simultaneously retaining advantages of net-shaping and enhanced properties, a process is needed which could be comprehensive on its own.

Powder injection molding (PIM) is ideal for fabrication of complex shapes in large quantities and has an advantage with costly materials due to reduced losses and easy recycling. Although the concept of PIM is 70 years old, the success in production is relatively recent [16]. These days powder injection molding is gaining extensive popularity due to the combination of net-shaping and performance [17]. Its success versus established processes like die-compaction, machining, and investment casting lies in producing intricate shapes at high production rates. Various authors [18–21] have processed niobium via powder metallurgy, but not much work (or none) has been done in the processing of pure niobium via PIM. An effort to apply powder injection molding to Nb-base superalloys was made in 1992 [22]. The final density achieved after sintering at 2350 °C was 94% of the theoretical density of niobium (8.57 g/cc).

The present work explores the processing of niobium via powder injection molding. The aim is to develop feedstock for niobium powder injection molding. This article identifies critical and optimum solids loading percentages based on rheological behavior of the feedstock and the proper processing window, based on the moldability index and simulation.

2. Experimental procedures

2.1. Powder and binder characteristics

Niobium powder Nb7 was acquired from Cabot Performance Materials, Boyertown, PA. Table 1 summarizes the characteristics of powder used in this study. Nb7 ($D_{50} \sim 7$ μm) was chosen, as powders having particle sizes between 0.5 and 20 μm are suitable for injection molding [17]. Fig. 1 shows the morphology of the powder used in the present work. The powder has irregular shaped particles with a broad particle size distribution, hence it will exhibit better shape retention during binder removal but lower packing density [22]. A wax–polymer binder was selected for this work. The binder consisted of paraffin wax, polypropylene, polyethylene, and stearic acid. Table 2 shows the characteristics of the binder components.

Table 1
Powder characteristics of Nb7 used in this study

Particle size (μm)		
D_{10}	D_{50}	D_{90}
3.7 ± 0.7	7.4 ± 0.6	12.4 ± 1.9
Densities (g/cm³)		
Apparent	Tap	Pycnometer
2.10 ± 0.03	3.00 ± 0.06	8.40 ± 0.12
Chemical composition (ppm)		
Carbon	Oxygen	Hydrogen
68	18,000	4000

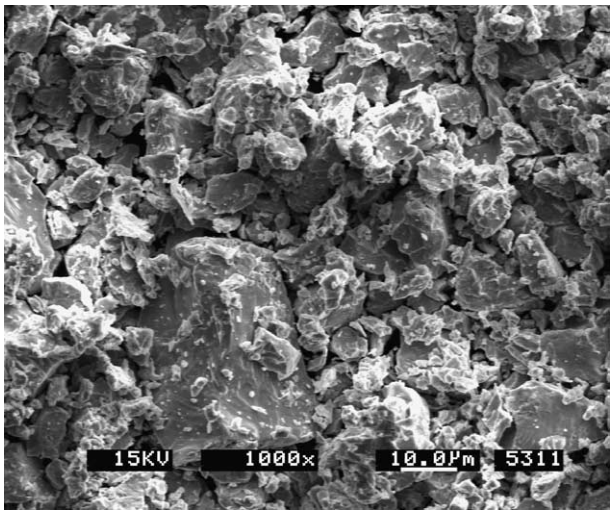

Fig. 1. Scanning electron micrograph of as-received niobium powder Nb7.

2.2. Feedstock mixing

PIM feedstock represents a balanced mixture of powder and binder [17]. The ratio of powder to binder largely determines the success or failure of subsequent processes. To make consistent products, homogeneous feedstock design is one of the important aspects of the PIM process. The solids loading and mixing methods are two important factors which determine the attributes of the feedstock. Solids loading is defined as the volumetric ratio of powder and binder [17]. The ratio at which powder particles are tightly packed and the binder fills all the voids between the particles is called the critical solids loading. The critical solids loading was measured using a torque rheometer (model: Rheocord 300p and Rheomex CTW 100p; supplier: Haake Corp., Paramus, NJ). A starting batch of 50 vol% solids loading was used and mixed at 150 °C in the rheometer. This equipment has a maximum chamber volume of 69 cm^3, and typically 65–75% of the volume is used for tests. The equipment is self calibrating as it reloads at a start of every new measurement. The appropriate amount of powder and binder were weighed out to produce a feedstock below the critical solids loading. Once the rheometer was heated to a programmed temperature, the binder components were added to the chamber and allowed to melt while being mixed at a programmed speed of 180 rpm. Next, the Nb powder was added to the binder and allowed to blend with the binders until the mixing torque stabilized, indicating a homogeneous feedstock mixture. Additional doses of powder were added, incrementing the solids loading by one percent each time and the torque was again allowed to stabilize, and this stable torque was observed. This procedure was repeated until the mixing torque either did not stabilize or rapidly increased, both indicating an excess amount of powder.

A proper selection of the mixing method is the key to achieve a homogeneous mix which is free of agglomerates, with an optimal content of powder and binder. High shear rates are required to smear and knead binder between the powders close to critical solids loading [23]. Therefore, low shear batch mixing routes such as sigma blade or double planetary mixing is avoided. Compounding of powder and binder was carried out in a twin shaft, co-rotating mixer (model: Continuous Processor; supplier: Readco Manufacturing Inc., York, PA). A flat paddle was used for maximum shearing. Compounding parameters are shown in Table 3. After compounding, the feedstock was granulated in a rotary feedstock granulator.

2.3. Feedstock property measurement

A homogeneous filling of feedstock into the mold depends on viscous flow of the mixture into the die cavity, and this requires certain rheological properties [23,24]. Stability in viscosity is one of the most important feedstock characteristics. The viscosity of the feedstock was measured using a capillary rheometer (model: Galaxy V 8052; supplier: Kayeness, Morgantown, PA). A heated cavity is used to melt the feedstock and it is forced through a die with a ram, while the ram rate, ram force, and time are recorded. The cavity of the

Table 3
Processing parameters of twin screw commotions compounding

Feeder speed (cm/min)	180
Processor speed (rpm)	200
Zone 1 (°C)	150
Zone 2 (°C)	165
Zone 3 (°C)	165
Zone 4 (°C)	150

Table 2
Characteristics of binder components used in binder system

Binder	Paraffin wax	Polypropylene	Polyethylene	Stearic acid
Vendor	Dussek Campbell	PolyVISIONS	DuPont	Fischer Scientific
Density (g/cm^3)	0.90	0.90	0.92	0.94
Melting range (°C)	42–62	110–150	60–130	74–83
Melting peak (°C)	58	144	122	79
Decomposition range (°C)	180–320	350–470	420–480	263–306

rheometer has been preheated to 140, 150, and 160 °C for feedstocks with solid loading percentages of 53%, 55%, 57%, and 59% to measure viscosity variation and to verify the critical solid loading percentage. A die diameter of 2 mm and a die length of 30 mm was selected and three tests were done at each temperature with variable ram rate (4–12 mm/min). A melt time of 300 s was selected for each test. Tests were also conducted at a constant shear rate of 2000 s^{-1}. Fig. 2 shows the overall procedure for developing feedstock covered through Sections 2.1–2.3.

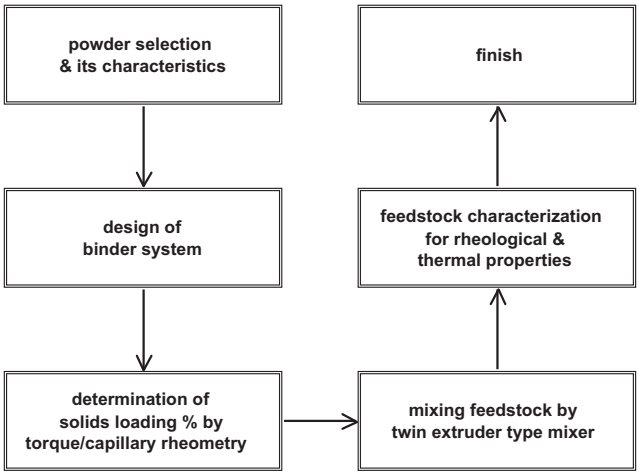

Fig. 2. Diagram for making PIM feedstock.

2.4. Injection molding

The feedstock was molded on a 30-ton reciprocating screw injection molding machine (model: 270V; supplier: ARBURG, Inc., Newington, CT). Fig. 3 shows an injection molded tensile bar and meshed geometry for simulation with its dimensions. The molding parameters are shown in Table 4.

Table 4
Molding parameters for niobium tensile bars

	Parameters		
Temperature profile			
Nozzle (°C)	135	Shot size	10 cm^3
Barrel zone 2 (°C)	140	Back pressure	0.5 MPa
Barrel zone 3 (°C)	150	Cooling time	14 s
Barrel zone 4 (°C)	150		
Barrel zone 5 (°C)	155		
	Step 1	Step 2	Step 3
Injection profile			
Speed (cm^3/s)	15.0	10.0	5.0
Pressure (bar)	500	450	450
Cutoff (cm^3)	3.0	2.5	2.0
Packing profile			
Pressure (bar)	450	300	200
Time (s)	2	1	1

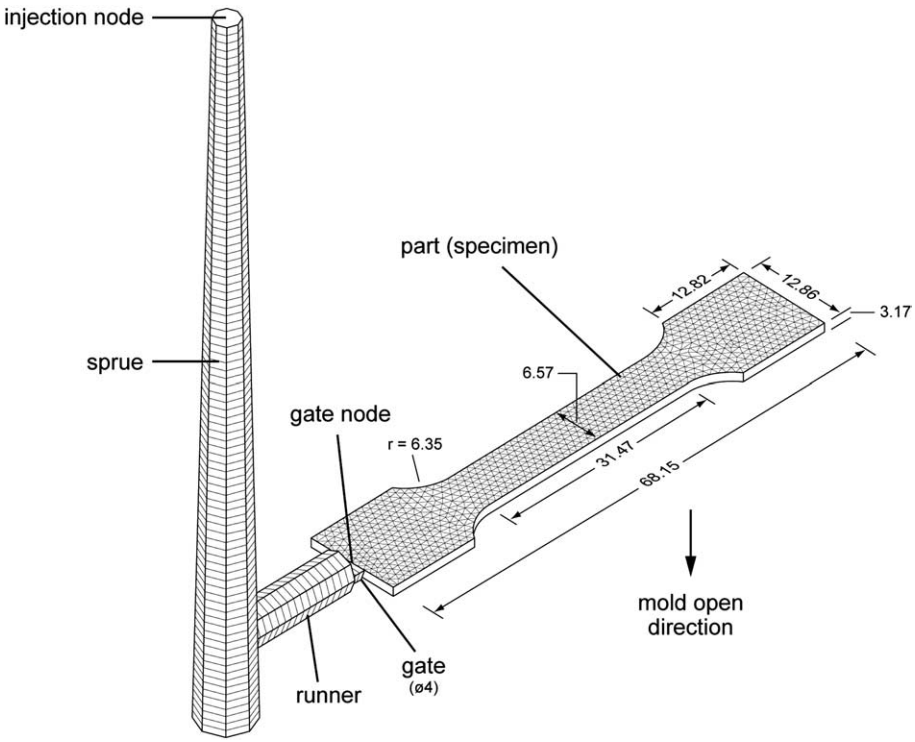

Fig. 3. Injection molded part and geometry of sprue, runner, gate and tensile test sample. All dimensions are in millimeters.

3. Simulation

3.1. Physical modeling

Simulation of the filling stage requires analysis of the flow and heat transfer during the entire mold filling stage. During such calculations, the computational domain varies with time. In the present section, the physical model of the mold filling stage is described in terms of a pressure-governing equation based on the momentum and mass conservation, and a temperature-governing equation based on the energy conservation.

The thickness of injection-molded parts is usually small compared with the other dimensions. The momentum equation can be approximated as a Hele-Shaw problem [25].

$$-\frac{\partial P}{\partial x}+\frac{\partial}{\partial z}\left(\eta\frac{\partial u}{\partial z}\right)=0$$
$$-\frac{\partial P}{\partial y}+\frac{\partial}{\partial z}\left(\eta\frac{\partial v}{\partial z}\right)=0 \quad (1)$$

Here P is the pressure, x, y, and z the local coordinates, u and v the velocities in the x- and y-direction, and η the viscosity as a function of a generalized shear rate and temperature. The coordinate system and velocity field in flow during mold cavity filling is illustrated in Fig. 4. In accordance with the Hele-Shaw approximation, the energy equation can be simplified as follows:

$$\rho C_p\left(\frac{\partial T}{\partial t}+u\frac{\partial T}{\partial x}+v\frac{\partial T}{\partial y}\right)=k\frac{\partial^2 T}{\partial z^2}+\eta\dot{\gamma}^2 \quad (2)$$

where T, t, ρ, C_p, k, and $\dot{\gamma}$ indicate the absolute temperature, the time, the melt density, the specific heat, the thermal conductivity, and the shear rate, respectively [26].

3.2. Rheological model of feedstock

The rheology of the feedstock can be expressed by a simple power law model with consideration of temperature dependency as [27,28]:

$$\eta(\dot{\gamma},T)=B\exp\left[\frac{E}{RT}\right]\dot{\gamma}^{n-1} \quad (3)$$

where n, B, E, and R indicate the power-law exponent, a material specific reference factor (some authors call this the reference viscosity), the flow activation energy for the Arrhenius temperature dependence of the viscosity, and the gas constant, respectively.

3.3. Numerical method

Numerical analysis of the mold filling stage of powder injection molding requires solution of both, the pressure equation (1) and the energy equation (2) during the entire filling cycle until the mold cavity becomes completely filled. A finite element method is employed to solve Eq. (1) while a finite difference method is used in the z-direction making use of the same finite elements in the x–y plane for solving Eq. (2). An automatic update of finite elements filled with feedstock is achieved by introducing a scalar fill factor indicating the degree of filling for each finite element node [29].

4. Results and discussion

4.1. Torque rheometer

The solids loading is defined as volumetric ratio of solid powder to the total volume of powder and binder. At critical solids loading with classical torque behavior, the mixing torque increases significantly and becomes erratic due to interparticle friction. Fig. 5 shows the variation of mixing torque with time for Nb7 as solids loading is incrementally increased. There is an increase in the torque with each powder addition, but torque does not become erratic. In a typical PIM feedstock with spherical powders, particles are tightly packed and the binder fills all the voids between the particles at critical solids loading. Nb7 powder has irregularly shaped particles, due to which torque increases with an increment in powder loading, but stabilizes because of angular shape, as there are no point contacts between the

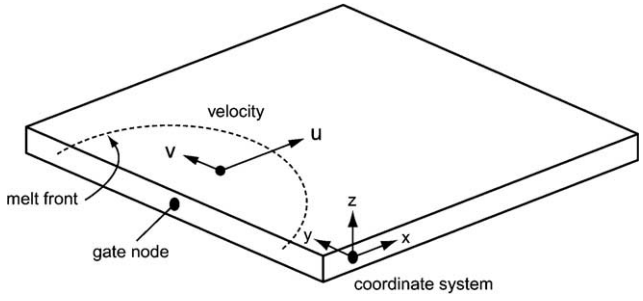

Fig. 4. Schematic diagram for coordinate system and velocity field in filling stage.

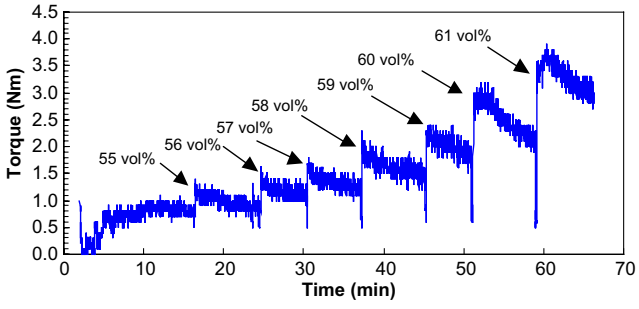

Fig. 5. Solids loading determination of the Nb7 feedstock.

particles. Because of this "non-classical torque behavior" it was difficult to determine the critical solids loading of the feedstock.

4.2. Capillary rheometer

To determine the critical solids loading and to study the rheological behavior simultaneously, capillary rheometry was used. In a capillary rheometer, the fluid is forced by a piston through the capillary. Under conditions of steady flow and from the measurement of the pressure drop and volumetric flow rate through the capillary, the shear stress and shear rate can be determined, from which the viscosity can be calculated. If the fluid is a Newtonian fluid, the velocity profile across the capillary is parabolic. The shear stress, shear rate, and viscosity at the wall for a Newtonian fluid are given by

$$\tau_w = \frac{\Delta P R_c}{2L} \tag{4}$$

$$\dot{\gamma}_a = \frac{4Q}{\pi R_c^3} \tag{5}$$

$$\eta_a = \frac{\tau_w}{\dot{\gamma}_a} \tag{6}$$

where τ_w, $\dot{\gamma}_a$, η_a, R_c, ΔP, L, and Q indicate the shear stress at the wall, the shear rate at the wall for a Newtonian fluid or apparent shear rate, the apparent viscosity, the capillary radius, the pressure drop across the capillary, the capillary length, and volumetric flow rate, respectively.

For non-Newtonian fluids, the velocity profile is not parabolic and the shear rate at the wall needs to be corrected as follows [30]:

$$\dot{\gamma}_w = \frac{\dot{\gamma}_a}{4}\left(3 + \frac{d(\log \dot{\gamma}_a)}{d(\log \tau_w)}\right) \tag{7}$$

where $\dot{\gamma}_w$ is the true shear rate at the wall. Eq. (7) is the well-known Rabinowitsch equation [30]. It is necessary to make measurements at several shear rates at a constant temperature. The viscosity of a Newtonian fluid does not change with the shear rate, and the value of the true shear rate is the same as the apparent shear rate. The viscosity of a pseudoplastic fluid like a PIM feedstock decreases with increasing shear rate, and the true shear rate is greater than the apparent shear rate. The amount of deviation in the true shear rate from the apparent shear rate indicates the degree of shear sensitivity.

See the curve fittings for the power model: the dependence of rheological behavior on temperature (Fig. 6); the dependence of rheological behavior on shear rate (Fig. 7); the feedstock homogeneity–viscosity variation with time (Fig. 8).

Table 5 details the parameters and errors related to the feedstock viscosity model. The slope of the viscosity

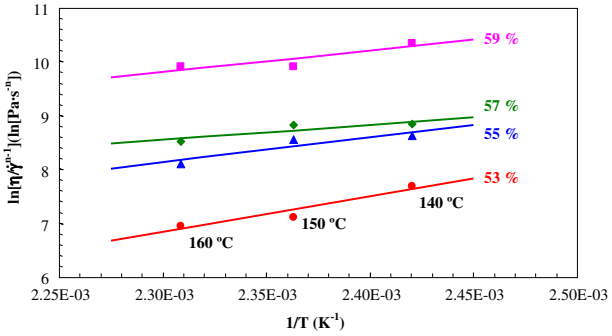

Fig. 6. The dependence of rheological behavior on temperature.

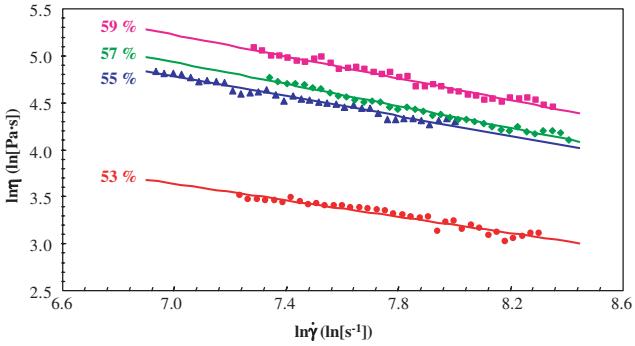

Fig. 7. The dependence of rheological behavior on shear rate.

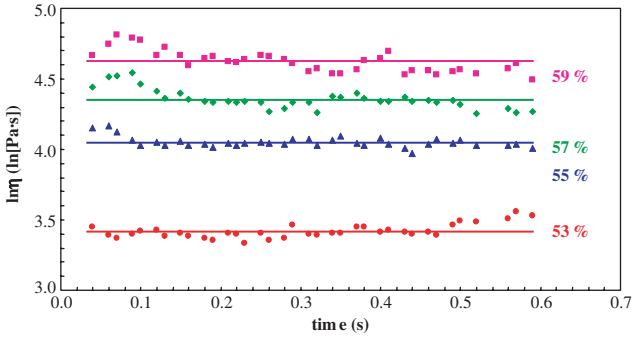

Fig. 8. Feedstock homogeneity: viscosity variation with time.

dependence on the shear rate (Fig. 6) gives the power law exponent n. It decreases with increasing solids loading. The lower the value of n, the higher the shear sensitivity, and hence the viscosity decreases faster with increasing shear rate. The temperature dependence of the viscosity may have an effect on the response of the material to the sudden non-uniform cooling within the cavity. During the molding stage, the feedstock is forced into a mold cavity where it immediately begins to cool. If the cooling is accompanied by a rapid increase in viscosity, the result may be distortion and cracking in the molded parts. Hence, weaker temperature dependence is desired to minimize problems due to a fluctuating

Table 5
Parameters and errors related to the feedstock viscosity model

Solids loading (%)	59	57	55	53
n	0.3403	0.4397	0.4635	0.5082
B (Pa · s)	2.067	13.56	8.648×10^{-2}	2.362×10^{-4}
E (kJ/mol)	32.83	21.50	38.22	54.90
Maximum B (kJ/mol)	2.782	16.69	9.985×10^{-2}	2.721×10^{-4}
Minimum B (kJ/mol)	1.681	11.90	7.856×10^{-2}	2.169×10^{-4}
Variation of B (%)	53.24	35.38	24.62	23.37
Average error (%)	2.412	1.247	1.895	2.678
Maximum error (%)	7.305	4.836	5.473	6.855

molding temperature—thereby minimizing stress concentration, cracks, and shape distortion. The flow activation energy E, calculated from the slope of viscosity dependence on the temperature graph (Fig. 7) decreases from 53 towards 57 vol% solids loading, and increases after that (Table 5). Fig. 8 gives the viscosity variation with time at a constant shear rate of 2000 s^{-1}, hence defining the feedstock homogeneity. The variation in the reference factor B is calculated from its maximum and minimum values (Table 5), which are obtained from corresponding maximum and minimum viscosity [31]. The higher the % variation in B, the lower the feedstock homogeneity. With an increase in solids loading percentage the feedstock becomes more inhomogeneous, depicting a higher powder–binder separation. This is because of the excess powder in a higher solids loading feedstock that leads to voids in green parts.

4.3. Critical and optimum solids loading percentage

With the above calculated parameters (n, E, and B) from the viscosity dependence graphs, it was possible to determine a window for critical solids loading (see Fig. 9). The graph shows a region of inflection at 57–58 vol% solids loading. In this region there is a sudden change in each rheological parameter (n, E, and B). This region can be termed as critical solids loading region where the particles are in contact with each other, and binder fills the space in between with no voids. At *critical* solids, loading the feedstock has a very high viscosity, therefore, slight excess binder is used to provide lubricity for molding [17]. This is termed *optimal* solids loading. 57 vol% was found to be the optimal solids loading percentage for powder injection molding the used niobium feedstock.

4.4. General moldability index

In the above determination of the optimal solids loading each parameter was not only calculated separately but also plotted on different axis. Also, lower solids loading feedstock has a higher shear sensitivity (n), which makes the determination of optimal solids loading difficult. To evaluate the general rheological properties of the feedstock a moldability index has been introduced, α_{stv}, which is defined as

$$\alpha_{stv} = \frac{1}{\eta_0} \frac{\left|\frac{\partial \log \eta}{\partial \log \dot{\gamma}}\right|}{\frac{\partial \log \eta}{\partial (1/T)}} = \frac{1}{\eta_0} \frac{1-n}{E/R} \tag{8}$$

where η_0 is the reference viscosity at 150 °C and a shear rate of 1000 s^{-1}. The subscripts s, t, and v of α_{stv} represent the effect of shear sensitivity, temperature sensitivity, and viscosity, respectively. The higher the value of

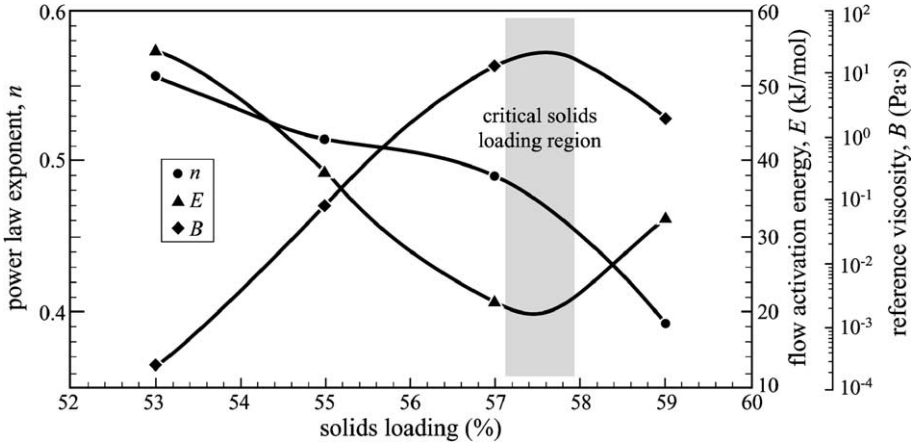

Fig. 9. Determination of the critical solids loading region.

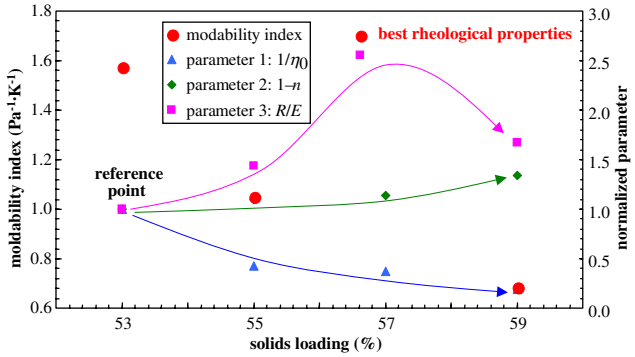

Fig. 10. General moldability index vs. solid loading %.

α_{stv}, the better the general rheological properties. Fig. 10 shows the general moldability index vs. solids loading.

As seen in this figure, the highest moldability index is at 57 vol% solids loading. The three parameters ($1/\eta_0$, $1/n$, and R/E) are also plotted against the solids loading percentage. There is a sharp increase in the parameter R/E at 57 vol%, then it decreases towards 59 vol%. This signifies that at 57 vol% solids loading feedstocks exhibit the lowest temperature sensitivity. Therefore, it can be concluded that at 57 vol% solids loading the feedstock has the best general rheological properties and is most suitable for injection molding.

4.5. Injection molding and processing window

Fig. 11 depicts the filling pattern during injection molding from simulation. It gives the filling time in seconds at various positions in the part during injection molding. Fig. 12 shows the optimum and maximum filling times for an injection temperature of 170 °C; the filling time is plotted against the injection pressure. It can be seen that the shorter the filling time, the higher the required injection pressure. As the filling time is increased beyond the pressure minimum at 1.3 s, there is a slight increase in injection pressure. This occurs due to heat transfer through the die wall, which results in formation of a thick frozen layer narrowing the actual flow channel. It is concluded that there is an optimal filling time, where minimum pressure is required to mold the part. At a filling time of 1.3 s, the lowest injection pressure is required, resulting in lower residual stresses. The maximum filling time was found to be 7.0 s, just before freezing in the flow channel would prevent a complete filling of the cavity. This concept has been applied to every temperature within the process range. It was observed that a higher injection temperature gives a longer maximum filling time, which is obvious due to later freezing in the flow channel [32]. The optimum filling time was observed to decrease with an increase in temperature. This occurs because of a higher temperature gradient

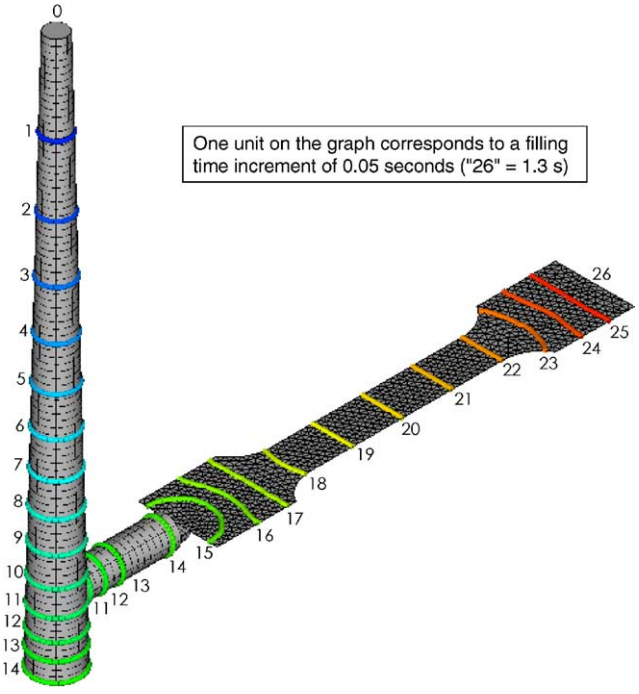

Fig. 11. Simulation result for filling pattern with filling time of 1.3 s and injection temperature of 170 °C.

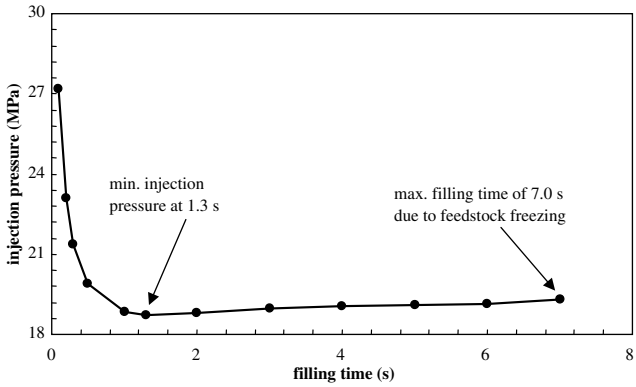

Fig. 12. Optimum and maximum filling times for injection temperature of 170 °C.

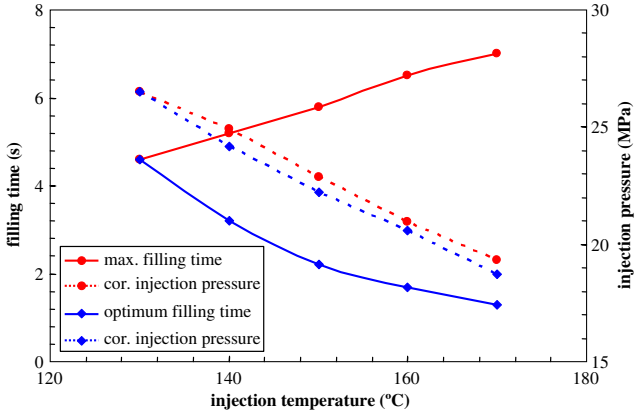

Fig. 13. Optimum and maximum filling times and corresponding injection pressures for various injection temperatures.

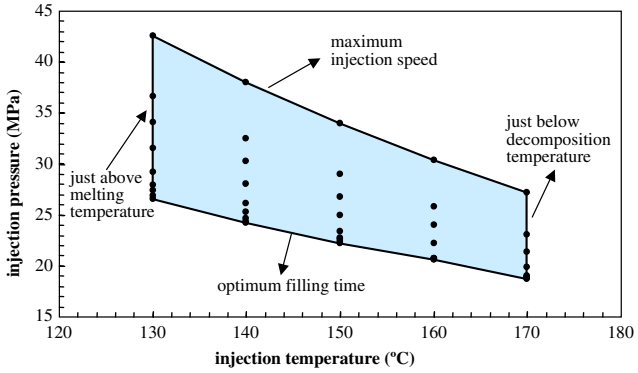

Fig. 14. Possible processing window area based on simulation.

between injection temperature and mold wall temperature. Therefore, it was found that a higher temperature gives a wider range of filling time. Fig. 13 shows the optimum and maximum filling times, and corresponding injection pressures for various injection temperatures.

From these calculations of optimal filling time and corresponding injection pressure and temperature, a processing window can be formulated. Fig. 14 gives that processing window for the Nb7 feedstock, depicting the injection pressure at various processing temperatures for the optimum filling time.

5. Conclusions

A systematical approach has been carried out to develop feedstock for niobium powder injection molding. Based on the rheological properties and simulation, it has been demonstrated for the first time that pure niobium powder can be injection molded. The niobium feedstock exhibited non-classical torque rheometry behavior due to irregular particle shape. Critical and optimal solids loading percentages were determined based on the rheological behavior of the feedstock. A sudden change in rheological parameters (n, E, and B) was observed at 57–58 vol% solids loading. This region can be termed as critical solids loading region. A moldability index (α_{stv}) has been used to evaluate general rheological properties and thereby determining optimal solids loading. At 57 vol%, the feedstock exhibited best rheological properties, and therefore was identified to be most suitable for injection molding. A processing window for injection temperature and pressure was formulated based on numerical simulations.

This is the first known attempt to determine the optimal solids loading based on rheological behavior of the feedstock. Future efforts will involve debinding and sintering of green injection molded parts. A process window for debinding and sintering will be determined based on density and impurity contents in the final sintered part.

Acknowledgements

The authors gratefully acknowledge the Ben Franklin Technology Development Authority for funding this research through the Center for Innovative Sintered Products. Furthermore, this research benefited from helpful suggestions of Dr. Sundar Atre.

References

[1] Cunningham LD. Columbium (Niobium) Tantalum 1996:1–5.
[2] Tolley RJ. The world's principal tantalum and niobium mines. Tantalum–Niobium Int Study Centre Bull 1991;35:3–4.
[3] Tither G. Progress in niobium markets and technology. In: International symposium niobium 2001, Orlando, Florida, 2–5 December 2001, TMS. p. 1–25.
[4] Collins LE. Processing of niobium-containing steels by steckel mill rolling. In: International symposium niobium 2001, Orlando, Florida, 2–5 December 2001, TMS. p. 527–42.
[5] Patel SJ, Smith GD. The role of Niobium in wrought superalloys. In: International symposium niobium 2001, Orlando, Florida, 2–5 December 2001, TMS. p. 1081–102.
[6] North B. Tantalum carbide and niobium carbide in hard metals. In: International symposium on tantalum and niobium, Goslar, Germany, 25–28 September 1995. Tantalum and Niobium International Study Center. p. 485–92.
[7] Togerson RT. Development of columbium alloys for re-entry vehicle structures. In: AIME-ASM Pacific Northwest Metals and Minerals Conference, Seattle, Washington, 26–28 April 1962. p. 2.
[8] Deutschmann L et al. Thin films of niobium and niobium oxides by PECVD. Eur J Solid State Inorg Chem 1991;28:1161–71.
[9] Gerfin T, Graetzel M. Ellipsometric investigation of metal-organic chemical vapor deposition of niobium oxide films. In: Chemical vapor deposition of refractory metals and ceramics III, Pittsburgh, PA. 363: MRS. p. 45–50.
[10] Pozdeev Y. Reliability comparison of tantalum and niobium solid electrolyte capacitors. Quality Reliab Eng Int 1998;14:79–82.
[11] Fischer V et al. Niobium as a new material for electrolyte capacitors with nanoscale dielectric oxide layers. In: Seventh International Conference on Properties and Applications of Dielectric Materials, Nagoya, Japan. 2003, IEEE. p. 1134–7.
[12] Frank RG. Refractory metal alloys. Proceedings of the symposium on refract metal alloys, metal and technology. Washington, DC: Plenum Press; 1968. p. 325–72.
[13] Wojcik CG. Processing, properties, and applications of high temperature niobium alloys. In: MRS Symposium, 1994. 322: Materials Research Society, Pittsburgh, PA. p. 519–30.
[14] Sandim HRZ, Padilha AF. On sinterability of commercial purity of niobium. Key Eng Mat 2001;189–191:296–301.
[15] Wojcik CG. Thermomechanical processing and properties of niobium alloys. In: International symposium niobium 2001, Orlando, Florida. 2–5 December 2001, TMS. p. 163–73.
[16] German RM, Cornwall RG. Powder injection molding: year 2000 market and industry report. Int J Powder Metall 2001;37:40–4.
[17] German RM, Bose A. Injection Molding of Metals and Ceramics. Princeton, NJ: Metal Powder Industries Federation; 1997.
[18] Balke CW. Pure Columbium. In: 85th General Meeting of Fansteel Metallurgical Corporation, Milwaukee, WI. 14 April 1944. Electrochemical Society, New York, NY. p. 89–95.
[19] Klopp WD, Sims CT, Jaffee RI. Vacuum Reactions of Niobium during Sintering. The symposium on columbium (niobium). Washington D.C.: John Wiley & Sons, Inc.; 1958. p. 106–20.

[20] Krehl M, Schulze K, Petzow G. The influence of gas atmospheres on the first stage sintering of high-purity niobium powders. Metall Trans A 1984;15A:1111–6.
[21] Levinskii YV et al. Interrelationship between properties of powders, the pressing and sintering conditions and structure of porous niobium. III. The porous structure of material of sintered niobium powders. Soviet Powder Metall Metal Ceram 1990;322:519–30.
[22] Schwartzwalder K. Am Ceram Soc B 1984;28:459–61.
[23] Bigg DM, Barry RG. Rheological analysis as a tool to predict quality in powder injection molding. In: 56th annual technical conference, ANTEC, Brookfield Center, CT, 1998. p. 997–1000.
[24] Zhang T et al. Influence of rheological behavior of ceramic mixes on injection molding of ceramic compacts. J Am Ceram Soc 1990;73:2171–5.
[25] Hieber CA, Shen SF. J Non-Newtonian Fluid Mech 1980;7:1–32.
[26] Kwon TH, Ahn SY. Powder Technol 1995;85:45–55.
[27] Li Y, Huang B, Qu X. Viscosity and melt rheology of metal injection molding feedstocks. Powder Metall 1999;42:86–90.
[28] Chen X et al. Determination of phenomenological constant of shear-induced particle migration model. Comput Mater Sci 2004;30:223–9.
[29] Wang KK, et al. Injection molding project. Cornell University, Ithaca, 1974–1989.
[30] Rabinowitsch B. Z Physik Chem 1929;145A:1.
[31] Suri P et al. Numerical analysis of filling stage during powder injection moulding: effects of feedstock rheology and mixing conditions. Powder Metall 2004;47:137–43.
[32] Zheng R et al. Thermoviscoelastic simulation of thermally and pressure-induced stresses in injection moulding for the prediction of shrinkage and warpage for fibre-reinforced thermoplastics. J Non-Newtonian Fluid Mech 1999;84:159–90.